Article

Conformational Changes During the Gating of a Potassium Channel Revealed by Structural Mass Spectrometry

Sayan Gupta,[1,2] Vassiliy N. Bavro,[4,5] Rhijuta D'Mello,[1,2] Stephen J. Tucker,[4,5,*] Catherine Vénien-Bryan,[5,6,7]
and Mark R. Chance[1,2,3,*]
[1]Center for Synchrotron Biosciences
[2]Center for Proteomics and Bioinformatics
[3]Department of Physiology and Biophysics
Case Western Reserve University, Cleveland, OH 44022, USA
[4]Clarendon Laboratory, Department of Physics
[5]OXION Initiative, Sherrington Building
[6]Department of Biochemistry
University of Oxford, Oxford OX1 3PU, UK
[7]Present address: IMPMC-UMR 7590, CNRS, Université Paris 6 et Paris 7, IPGP, 75015 Paris, France
*Correspondence: stephen.tucker@physics.ox.ac.uk (S.J.T.), mark.chance@case.edu (M.R.C.)
DOI 10.1016/j.str.2010.04.012

SUMMARY

Potassium channels are dynamic proteins that undergo large conformational changes to regulate the flow of K$^+$ ions across the cell membrane. Understanding the gating mechanism of these channels therefore requires methods for probing channel structure in both their open and closed conformations. Radiolytic footprinting is used to study the gating mechanism of the inwardly-rectifying potassium channel KirBac3.1. The purified protein stabilized in either open or closed conformations was exposed to focused synchrotron X-ray beams on millisecond timescales to modify solvent accessible amino acid side chains. These modifications were identified and quantified using high-resolution mass spectrometry. The differences observed between the closed and open states were then used to reveal local conformational changes that occur during channel gating. The results provide support for a proposed gating mechanism of the Kir channel and demonstrate a method of probing the dynamic gating mechanism of other integral membrane proteins and ion channels.

INTRODUCTION

Ion channels are integral membrane proteins that regulate the selective flow of ions such as Na$^+$, K$^+$, and Cl$^-$ across the membrane, and thereby play an important role in the control of cellular electrical excitability and ionic homeostasis. In the prototypical potassium channel the passage of K$^+$ ions, however, the pore is governed by a "gate" that is opened and closed in response to a variety of regulatory stimuli (Swartz, 2004). Understanding the molecular mechanism of this dynamic gating

process is therefore critical to understanding the effects of inherited mutations on channel function, understanding how ligand binding regulates gating, and also understanding the molecular basis of drug action on channel function.

Over the last 10 years, a variety of K$^+$ channel structures have suggested that the mechanism of K$^+$ channel gating involves large conformational changes at the inner mouth of the pore. However, advances in our understanding have been limited by a lack of structural information for a specific channel poised in both open and closed conformations. High-resolution structures are now available for both eukaryotic (Nishida et al., 2007; Tao et al., 2009) and bacterial members of the inwardly rectifying (Kir) potassium channel family (Kuo et al., 2003). But all of these structures appear to be in closed states and no high-resolution structure for an open state has so far been available. For KirBac3.1, medium resolution structural models of an open state have been proposed based on both cryo-electron microscopy and AFM studies of 2-D crystals of KirBac3.1, however, these data lack important details implicating specific domains in channel gating (Jaroslawski et al., 2007; Kuo et al., 2005). Therefore, the ability to examine KirBac3.1 in these two different conformations makes it a very attractive candidate for investigating the structural differences between open and closed states of the channel.

Radiolytic labeling by synchrotron X-rays combined with mass spectrometry is ideally suited to revealing the conformational dynamics and specific side chains involved in ion channel gating (Takamoto and Chance, 2006; Xu and Chance, 2007). Similar labeling of membrane proteins can also be achieved by the direct chemical production of such radicals, but these approaches have restricted temporal resolution and limited radical accessibility (Zhu et al., 2009). By contrast, in this method, high flux X-rays interact with water to produce hydroxyl radicals with millisecond timescale exposures to label dilute solutions of purified proteins. Hydroxyl radicals rapidly react with solvent accessible residues and undergo oxygen-dependent covalent modifications that are analyzed by high-resolution mass spectrometry to probe the sites and extent of modification (Takamoto
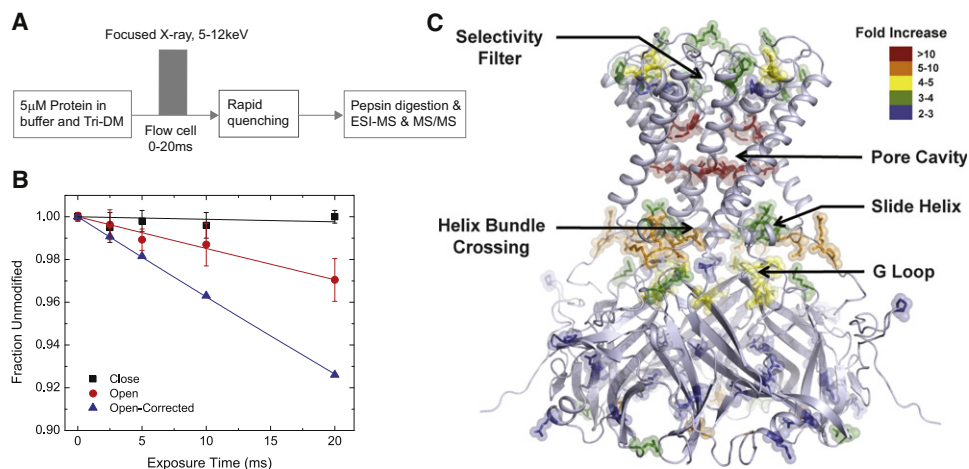
Figure 1. Radiolytic Labeling Identifies Residues in KirBac3.1 with Increased Modification Rates in the Open State.
(A) Experimental scheme. Dilute buffered solution of closed and open KirBac3.1 in TriDM detergent were irradiated with a focused synchrotron X-ray beam for 0–20 ms in a flow set-up for radiolytic labeling of the solvent accessible amino acid side chains. The exposed protein solution was rapidly quenched to stop secondary free radical reactions. The detergent was removed and controlled pepsin digestion was carried out to obtain peptide fragments of 4–10 amino acids. Reverse phase chromatography was used to separate the peptides and ESI-MS and MS/MS carried out to quantify the extent and identify site of modification.
(B) Dose response plot. A representative dose response plot for peptide, 120-GML*GL*AVAASLI-131 (*indicates modification identified by MS/MS). The closed and open states of KirBac3.1 were prepared in buffer containing 50 mM Mg^{2+} and 1 mM EDTA respectively. EDTA is an •OH radical scavenger and reduces the X-ray dose by a factor of ∼2.5 (Figure S3). The observed rate constant k_{open} is corrected and $k_{open-corrected}$ is compared with that of k_{closed} (Table 1). The solvent accessibility of L122 and L124 at the cavity of membrane pore are increased by a factor of ∼31 from close to open state of KirBac3.1. Rates were calculated for all the modified peptides and compared between the closed and open states to obtain information on conformation dynamics. Error bars represent standard deviation between experimental repeats.
(C) Mapping the solvent accessibility changes. Modified residues are represented by sticks on the X-ray crystal structure of KirBac3.1 in the closed state (PDB 1XL4). The color codes indicate the changes in rates of modification or solvent accessibility on transition from the closed to open state. Only the residues with >2-fold increase are highlighted.

and Chance, 2006; Xu and Chance, 2007). Thus, residues in an ion channel that have increased interactions with solvent due to changes in the structure of the channel in an open state will have dramatically increased labeling efficiency in comparison to their rate of modification in a closed state. Such analysis not only has the potential to highlight those residues that form the permeation pathway of the channel, but also can identify residues that mediate the gating process through conformational rearrangements. Recently, we have used a similar approach to probe the allosteric activation of the GPCR rhodopsin (Angel et al., 2009a; Angel et al., 2009b). In this study, we have applied this method to KirBac3.1 and now demonstrate that it can also be used to reveal details of ion channel gating dynamics, and therefore has the potential to be adapted for the study of other ion channels

RESULTS AND DISCUSSION

Radiolytic Labeling as a Tool for the Analysis of Local Conformational Changes in KirBac3.1
We subjected purified KirBac3.1, stabilized in either open or closed states, to millisecond pulses of focused synchrotron X-rays using a flow cell and rapidly quenched the sample to reduce the secondary radical chain reactions (Figure 1A)(Xu and Chance, 2007; Xu et al., 2005). After X-ray exposure, the protein samples were digested by pepsin and then analyzed by liquid chromatography (LC) coupled to mass spectrometry (see Figure S1A available online). Typical mass spectrometric

sequence coverage was 92% (Table 1; Figure S2). The extent of modification was quantified after extraction of LC ion current data for unmodified and modified peptides of interest (Figure S1A; Experimental Procedures). KirBac3.1 exposed to X-rays in repeated experiments exhibited consistently similar extent of radiolytic labeling on the same residues. Sequence identities of peptides and specific sites of oxidative modification were confirmed by MS/MS (Figure S1B). The extents of modification were plotted against irradiation time and the rates of modification determined from X-ray dose response plots in triplicate experiments (Figure 1B). The rates of modification for all peptides observed are summarized in Table 1.

The use of LC coupled mass spectrometry to quantify the extent of modification coupled with MS/MS to identify the specific residues involved provides a quantitative measure of solvent accessibility with high structural resolution (Guan and Chance, 2005; Kiselar et al., 2002). However, the relative reactivity of a residue is governed by its intrinsic reactivity as well as solvent accessibility. Thus, the most informative comparisons are those that compare specific residues in specific peptides across conformational states, e.g., open versus closed. Also hydroxyl radicals are generated by radiolysis isotropically wherever water is present, thus when water is in contact with side chain residues, they become targets for labeling.

An advantage of this study is that we have a high-resolution structure of the closed state (Kuo et al., 2003), thus we can interpret the radiolytic labeling by comparing the relative solvent accessibility of modified residues in the open state to their rate

of modification in the closed state (Figure 1C). Those residues identified with significant increases in their modification rate in the open state are therefore likely to be involved in the dynamic conformational changes that mediate opening of the channel pore.

Structural Changes in the Transmembrane/Pore Domain During Gating

The largest change in rate of modification from the closed to the open state is seen for peptide 120–131, where residues L122 and L124 show a 31-fold increase (Figure 1B). Residues L122 and L124 are located on the inner pore-lining TM2 helix (Figure 2A), and their rate of modification provides direct evidence to support current models of K$^+$ channel gating in which these helices move apart at the "helix bundle crossing" during channel opening to permit the flow of K$^+$ ions into the inner cavity (Swartz, 2004).

Peptide 89-94 exhibits the next largest change in modification, with residue M94 showing a 15-fold increase. This residue is located toward the base of the pore-loop helix and packs closely with G120 in TM2. Interestingly, there is now a growing body of evidence for a wide range of K$^+$ channels, including Kir channels, for the existence of an additional gate close to the selectivity filter (Ader et al., 2008; Berneche and Roux, 2005; Cordero-Morales et al., 2006). Although the rotational movement of the TM helices and opening of the pore cavity may be responsible for the change in accessibility of M94 in the open state, a number of other residues close to the selectivity (T84, D85, and F88 in the pore helix, and P107 and N110 at the top of TM2) also undergo changes in accessibility in the open state and are clustered at an intersubunit interface (Figure 2B and Table 1). Together these results are therefore consistent with a conformational change near the selectivity filter of KirBac3.1 that may be similar to the movements in the KcsA channel that occur during channel inactivation (Ader et al., 2008). Furthermore, the tight packing between M94 and G120 may also permit allosteric coupling of gating events at the helix bundle crossing with those occurring at the selectivity filter (Ader et al., 2008). We propose that these results provide strong evidence for the existence of gating mechanism located within or near to the selectivity filter of KirBac3.1.

Conformational Changes at the Membrane Interface

The conformational changes in TM2 that result in the movement of the helix bundle crossing are representative of the gating motions thought to occur in all major classes of K$^+$ channel (Swartz, 2004). However, Kir channels possess other unique structural domains including the "slide-helix" and a large C-terminal domain that are also involved in channel gating (Kuo et al., 2003). In particular the slide-helix is thought to couple movement of the cytoplasmic domains to the TM/pore domains (Enkvetchakul et al., 2007). It is therefore of major importance that we also observed significant changes in the rate of modification at this potential gating interface. Residues K30, R31, L34, and D35 in the flexible linker that connects the N-terminus with the slide-helix exhibit an 8-fold increase in modification rate, and residues Y38 and L41 within the slide-helix itself exhibit a 4-fold change. In the closed-state structure these residues provide a range of inter- and intrasubunit contacts that are important

for maintaining the closed state of the channel (Figure 3A). One such interaction is with residue R167 within the CD loop of the cytoplasmic domain, and we also observe a 4-fold increase in reactivity of this residue. R167 is highly conserved and contributes to a charged cluster at the membrane-facing surface that is thought to be responsible for interaction with signaling lipids such as PIP$_2$ (Tucker and Baukrowitz, 2008). The CD loop has also been implicated in Kir channel regulation by cholesterol (Epshtein et al., 2009; Singh et al., 2009). It is therefore likely that lipid-gating of Kir channels is driven by modulation of intra- and intersubunit interactions in this region (Enkvetchakul et al., 2007; Tucker and Baukrowitz, 2008).

A Gate within the Cytoplasmic Domain?

In eukaryotic Kir channels the inner vestibule of the cytoplasmic domain is thought to provide a binding site for intracellular polyamines that become trapped at depolarizing potentials and thereby contribute the strong voltage dependency or "inward rectification" of these channels (Kuo et al., 2003; Nishida et al., 2007). However, KirBac channels do not appear to exhibit intrinsic rectification even in the presence of polyamines and so the functional role of this domain is not clear (Cheng et al., 2009). It is possible that it may serve as a site for regulation of the channel and it is known that several Kir channel regulators such as ATP and G-proteins directly bind to this domain to influence channel gating (Bichet et al., 2003). This suggests that these domains do not remain static during channel gating and that conformational changes must occur as the channel opens and closes. However, as yet there is very little direct evidence of what structural changes may occur.

The "G-loop" within the cytoplasmic domain is located next to the CD-loop and previous studies have shown that it has a major influence on Kir channel gating. It has also been proposed to represent a third class of structural "gate" within the Kir channel that is required to be in an open conformation to permit the flow of K$^+$ ions (Bichet et al., 2003; Nishida et al., 2007; Pegan et al., 2005). It is therefore highly significant that we identified several residues within the G-loop of KirBac3.1 (E248, F250, and V254) that also exhibit a 5-fold increase in rate of modification on channel opening (Figure 3A). These residues are also structurally close to P138 at the base of TM2 the adjacent subunit, which showed a 3-fold increase in rate of modification on gate opening (Figure 3A).

Intriguingly, only few residues within these loops of the cytoplasmic domain show major changes in accessibility, while most other residues exhibit only minor changes (shown in blue 2–3-fold changes) (Figure 3B). It has been proposed that the main β−sheet structures of the cytoplasmic domains present a rigid Ig-like domain (Fallen et al., 2009). Thus these core domains may not themselves undergo large allosteric changes during channel gating. Instead the major conformational changes occur at the interface between these domains, in their connecting loops (e.g., CD loop and G-loop) and at their interface with the TM/pore domain and slide-helix.

Conclusions

The data obtained in this study now allow us to propose a more detailed model of the major conformational changes that occur during Kir channel gating; this model is shown in Figure 4.

Table 1. Hydroxyl radical modification rate constant for residues in KirBac3.1

Sequence No.[a]	Sequence Modified residue(s)[b] SA[c]	No. of Modification Peaks Detected in TIC[d]	Rate Constant of Modification (s^{-1})[e] Close KirBac3.1 k_{close}	Open KirBac3.1 k_{open}	Ratio of Rate[f] $k_{open-corrected}/k_{close}$
16–26	NSDGSSNITRL	0	—	—	—
23–28	ITRLGL	0	—	—	—
29–41	E K[b] R[b] G W L[b] D[b] D H Y[b] H D L[b] K30, 149Å^2[c] R31, 89 Å^2 L34, 17 Å^2 D35, 25 Å^2 Y38, 18 Å^2 L41, 44 Å^2	Peak 1[g] K30,R31,L34,D35 Peak 2 Y38, L41	Peak 1 2.5 ± 0.3[h] Peak 2 7.7 ± 2.0	Peak 1 8.6 ± 1.0 Peak 2 11.3 ± 1.8	8.4 3.6
43–49	TVSWPVF	0	—	—	—
50–56	ITLITGL	0	—	—	—
53–57	ITGLY	0	—	—	—
57–63	YLVTNAL	0	—	—	—
64–67	FALA	0	—	—	—
64–69	FALAYL	0	—	—	—
74–83	V I E[b] N A R P G S F E76, 61 Å^2	1	12.7 ± 2.2	17.4 ± 2.7	3.4
84–88	T[b] D[b] A F F[b] T84, 44 Å^2 D85, 17 Å^2 F88, 21 Å^2	Peak 1 F88 Peak 2 T84,D85	Peak 1 3.6 ± 0.7 Peak 2 0.55 ± 0.09	Peak1 4.1 ± 0.8 Peak 2 1.00 ± 0.15	2.8 4.5
89–94	F S V Q T M[b] M94, 16 Å^2	1	0.08 ± 0.07	0.50 ± 0.10	15.3
95–101	ATIGYGK	0	—	—	—
103–112	I P I G P[b] L A N[b] T L P107, 86 Å^2 N110, 19 Å^2	1	0.7 ± 0.2	0.9 ± 0.1	3.2
113–118	VTLEAL	0	—	—	—
120–131	GML[b]GL[b]AVAASLI L122, 28 Å^2 L124, 24 Å^2	1	0.12 ± 0.17	1.50 ± 0.12	30.6
125–131	AVAASLI	0	—	—	—
132–135	YARF	0	—	—	—
136–143	T R P[b] T A G V L P138,3 Å^2	1	2.3 ± 0.5	2.9 ± 0.5	3.1
145–150	SSRMVI M148, 0 Å^2	0	—	—	—
148–153	MVISDF M148, 0 Å^2 F153, 5 Å^2	0	—	—	—
160–166	M[b] M[b] R L A N L M160, 19 Å^2 M161, 0 Å^2	Peak 1 M160 Peak 2 M161	3.1 ± 0.4 7.4 ± 0.8	2.8 ± 0.4 4.0 ± 0.6	2.2 1.3
167–174	R[b] I[b] E Q I I E A R167, 25 Å^2 I168, 102 Å^2	1	10.1 ± 1.0	15.4 ± 2.8	3.7
175–180	D[b] V[b] H L V L D175, 42 Å^2 V176, 0 Å^2	Peak 1 V176 Peak 2 D175	35.5 ± 4.3 8.8 ± 0.1	25.2 ± 0.6 9.9 ± 0.1	1.7 2.8

Table 1. *Continued*

Sequence No.[a]	Sequence Modified residue(s)[b] SA[c]	No. of Modification Peaks Detected in TIC[d]	Rate Constant of Modification (s^{-1})[e]		Ratio of Rate[f] $k_{open-corrected}/k_{close}$
			Close KirBac3.1 k_{close}	Open KirBac3.1 k_{open}	
181–192	V R S E[b] I S Q E[b] G M[b] V F E184, 22 Å^2 E188, 26 Å^2 M190, 90 Å^2	Peak 1 M190	6.6 ± 1.0	2.0 ± 0.3	0.7
		Peak 2 E184	9.8 ± 1.1	11.5 ± 2.3	2.9
		Peak 3 E188	6.9 ± 1.1	8.6 ± 1.6	3.1
192–200	F R R F H D[b] L T L D197, 48 Å^2	1	7.7 ± 1.1	7.7 ± 0.2	2.4
199–207	T L T R S R S P I	1 (+14) Unknown	1.3 ± 0.1	1.0 ± 0.2	1.9
209–212	SLSW W 212 - 6 Å^2	0	—	—	—
213–218	TVMHPI M215 - 22 Å^2	0	—	—	—
216–228	H P I D H H S P[b] I Y G E T P223 - 19 Å^2	Peak 1 P223	8.1 ± 1.3	17.6 ± 3.2	5.3
		Peak 2 Unknown	2.5 ± 0.1	2.2 ± 0.5	2.2
229–239	D E[b] T L R N S H S E[b] F E230, 119 Å^2 E238, 2 Å^2	Peak 1 E230	17.0 ± 2.5	19.3 ± 2.0	2.8
		Peak 2 E238	20.1 ± 1.7	18.4 ± 4.0	2.2
240–243	LVLF	0	—	—	—
243–263	FTGHHE[b]AF[b] AQNV[b] HARHAY[b] SCD[b] E248, 56 Å^2 F250, 4 Å^2 V254, 0 Å^2 Y260, 1 Å^2 D263, 25 Å^2	Peak 1 E248 F250 V254	1.5 ± 0.2	2.7 ± 0.2	4.4
		Peak 2 Y260 D263	2.2 ± 0.5	0.6 ± 0.1	0.7
265–271	I I W[b] G G H F W267, 74 Å^2 F271, 10 Å^2	1	32.2 ± 2.0	9.0 ± 0.2	0.7
272–275	VDVF	0	—	—	—
276–290	T T L P[b] D G R R A L D L G K F P279, 103 Å^2	1	4.5 ± 0.4	5.1 ± 1.2	2.8
276–301	TTLP[b] DGRRALDLGKFHEIAQHHHHHH P279, 103 Å^2 Other: multiple modification toward C-terminal–poly His region	Peak 1 P279	NR	NR	NR
		Peaks 2 and 3 Unknown	NR	NR	NR

NR, data not reported; SA, solvent accessibility; TIC, total ion chromatogram.

[a] Sequence coverage (92%) was obtained from the LC-MS analysis of pepsin fragments.

[b] Modified residue identified by MS/MS.

[c] The solvent accessibilities of individual side chains in KirBac3.1. The software, GETAREA 1.0 beta (http://curie.utmb.edu/getarea.html)(Fraczkiewicz and Braun, 1998) was used to calculate the solvent accessible surface area per residue from the PDB file 1xl4. The surface areas (in Å^2) for modified residues and highly reactive probe residues are shown.

[d] Total number of modification peaks (+14, +16, +4, etc.) observed in the selected ion chromatogram of the modified peptide fragment. Rates are calculated for individual peaks (Figure S1; Experimental Procedures).

[e] Rate constants were estimated by using a nonlinear fit of hydroxyl radical modification data to a first order decay as described in the Experimental Procedures.

[f] The closed and open states of KirBac3.1 were prepared in buffer containing 50 mM Mg^{2+} and 1 mM EDTA respectively. EDTA is an ·OH radical scavenger and reduces the X-ray dose by a factor of 2.45 (Figure S3; Experimental Procedures). The rate constant k_{open} is corrected by multiplying the factor 2.45 ($k_{open-corrected} = k_{open} \times 2.45$) and ratio of $k_{open-corrected}$ and k_{closed} was determined.

[g] Mixed modifications. A single modification peak is composed of multiple modified residues.

[h] Error in rate constant estimation calculated from nonlinear fit.
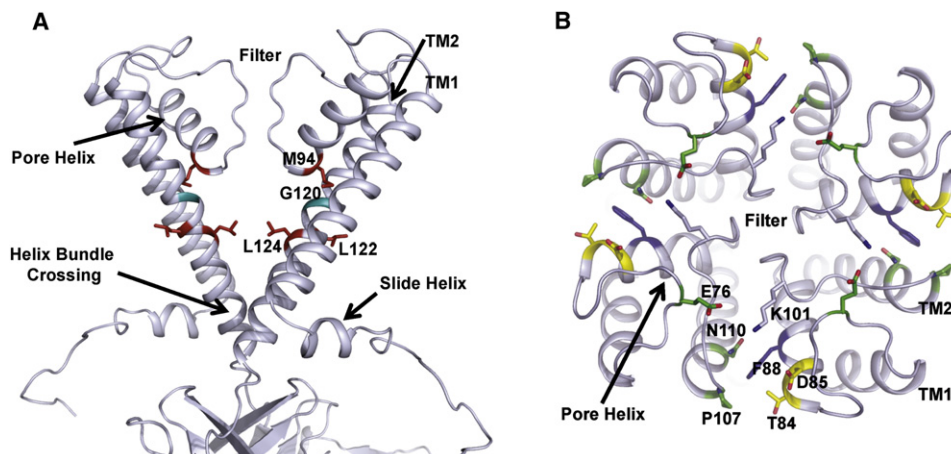
Figure 2. Modified Residues Highlight TM/Pore Domain Involved in KirBac Channel Gating
The color codes are the same as for Figure 1C and residues with elemental color scheme (cpk) are not modified but involved in close packing interaction with the modified residues.
(A) Conformational changes in TM2 and the pore-helix. For clarity only the TM section of two diagonally opposed monomers are shown. Note the proximity between M94 and G120 (the glycine gating hinge in TM2).
(B) Dynamic gating near the selectivity filter. Top-down view of the pore domain. Note the clustering of these modified residues at an intersubunit interface. Residue K101 forms an intersubunit salt bridge with modified residue E76 in the closed state conformation.

The principal movements involved are a translocation of the cytoplasmic domain upward to engage with the TM/pore domain and the slide-helix/N-terminus, and a rotational movement of the TM-helices to open the gate at the helix-bundle crossing. Our results also now provide direct evidence for a dynamic role of the G-loop and CD-loop during channel gating and are consistent with the potential role of the G-loop as an actual gate within the cytoplasmic domain. We have also been able to identify a number of conformationally sensitive residues near to the selectivity filter of KirBac3.1 that are consistent with the existence of an additional gating mechanism in the filter and

that merit future investigation in functional assays. Although we cannot confirm that these structural changes are identical to those that exist for in vivo gating of the channel, they provide very specific and testable predictions for mutagenesis and functional studies.

This study also demonstrates that radiolytic footprinting coupled with mass spectrometry can provide a powerful probe of ion channel gating dynamics, and has the potential to be applied to the gating mechanism of many other classes of ion channels and membrane proteins. Furthermore, future studies that combine such recent advances in radiolytic labeling coupled
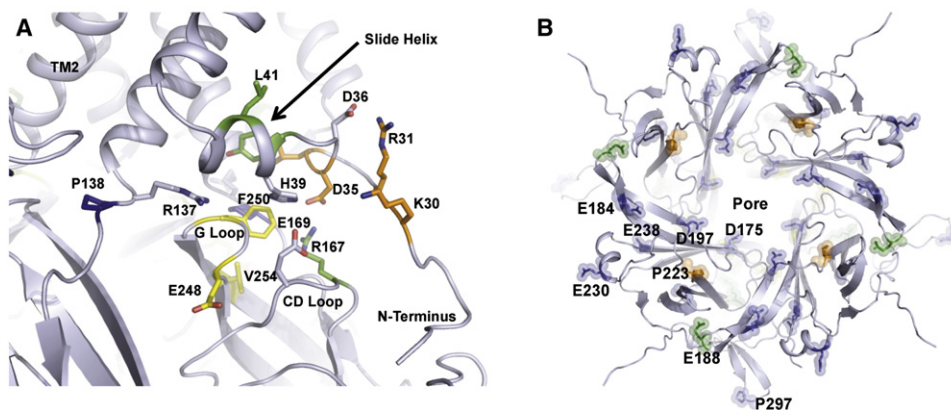

Figure 3. Modification of Residues at the Membrane Interface and Intracellular Domain
The color codes are the same as for Figure 2.
(A) A potential gating interface between the TM/pore domain and the cytoplasmic domain. Note the interaction between the modified residues and the G-loop/CD-loop and the slide-helix/N-terminal linker.
(B) Location of modified residues in the intracellular domain. Most of the residues identified in this domain show only minor changes in accessibility (shown in blue 2–3-fold changes) and may reflect the fact that the cytoplasmic domains do not undergo as large allosteric changes during channel gating as other domains (e.g., the slide-helix and TM2).
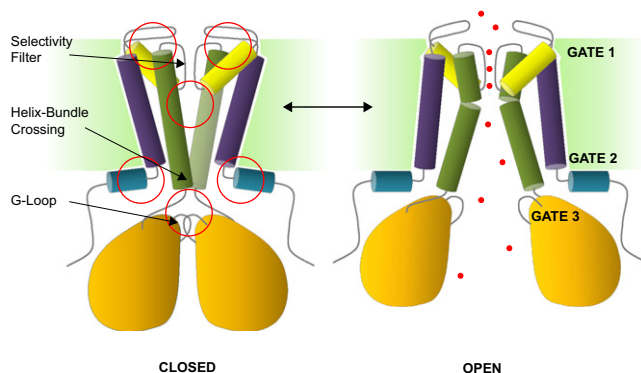
Figure 4. Proposed Gating Mechanism for Kir Channels

Taken together the modified residues provide a picture of the dynamic motions involved in the transition between the open and closed state and support the proposed existence of three potential gates within the channel. Shown are schematic views of KirBac3.1 in the closed (left) and open (right) states. The regions that show the largest conformational changes during channel gating are circled in the closed state.

to rapid O^{18} exchange mean this technique could also be used to probe channel gating processes in real time with millisecond resolution (Angel et al., 2009b).

EXPERIMENTAL PROCEDURES

Expression and Purification of KirBac3.1

A codon-optimized version of the KirBac3.1 from the α-proteobacterium *Magnetospirillum magnetotacticum* was synthesized (GenScript), and cloned into the pET30a vector (Novagen), with a C-terminal 6xHis-tag. BL21 Codon-Plus RP cells (Stratagene) were used for expression. The purification protocol was as described previously (Kuo et al., 2005), with the following exceptions: cell were grown at 19°C overnight after induction and the lysis buffer used was 50 mM Tris-HCl pH7.8, 150 mM NaCl, 50 mM KCl.

Preparation of Open and Closed State KirBac3.1 for Radiolysis

Two 100-μl samples of 3.7 μg/ml (30.8 μM) stocks KirBac3.1 in 50 mM Tris-HCl pH 8.0 containing 20% glycerol and 0.02% n-tridecyl-b-D-maltopyranoside (TriDM, Anatrace cat. no. T323LA) were individually diluted with 6× dialysis buffer 1 (50 mM MgCl₂, 150 mM KCl, 0.02% TriDM in 10 mM Na-Cacodylate buffer pH 7.0) and dialysis buffer 2 (1 mM EDTA, 150 mM KCl, 0.02% TriDM in 10 mM Na-Cacodylate buffer pH 7.0) to prepare closed and open KirBac3.1 respectively. The 600 μl of open and closed KirBac3.1 solution were dialyzed against 250 ml of dialysis buffer 1 and 2 respectively in Slide-A-Lyzers Mini Dialysis Units 3500MWCO. The dialysis step was repeated three times to remove the glycerol and Tris-HCl. All sample handing was done at 4°C.

Synchrotron X-ray Radiolysis

Open KirBac3.1 and closed KirBac3.1 in detergent were exposed to synchrotron X-ray white light at the National Synchrotron Light Source's (Brookhaven National Laboratory, Upton, NY) beamline X-28C operating at ring energy of 2.8 GeV. The X-ray beam parameters were optimized by using the standard fluorophore assay; this assay monitors the loss of intensity of an Alexa fluorophore to determine the effective hydroxyl radical concentration (Gupta et al., 2007). The effective hydroxyl radical concentration is 2.45 times less for open KirBac3.1 because of the presence of 1 mM EDTA (Figure S3). The high X-ray flux density generated by focusing the beam with a mirror (mirror angle to 5.5 mrad and the bender value to 8.0 mm) permits a sufficient dose to be delivered in a few milliseconds, reducing chemical noise and enhancing LC-MS data acquisition (Sullivan et al., 2008). KirBac3.1 samples were irradiated using a two-step flow method in a modified KinTek (KinTek Corporation) apparatus. In the first step, the 100 μl of sample was passed through a flow cell

with an irradiation cell volume of 3.5 ul. The flow speed was varied to generate X-ray irradiation time intervals ranging from 0 ms to 20 ms. In the second step the flow speed was adjusted such that the samples were collected in methionine-amide (final concentration of 10 mM) in 30 ms to rapidly quench any peroxide-induced or free radical-induced secondary oxidations during the post exposure period. All exposures were carried out at 10°C. Samples were frozen in dry ice and stored at −80°C before proteolytic cleavage and liquid chromatography and mass spectrometric analysis (LC-MS).

Removal of Detergents and Protease Digestion of KirBac3.1

Detergent was removed from protein samples after X-ray exposure by methanol-water-chloroform precipitation. 400 μl of methanol was added to 100 μl (~20 μg) of irradiated samples and mixed thoroughly for 1 min. 300 μl of chloroform was added and mixed thoroughly for 1 min. 300 μl of water was added and mixed thoroughly for 1 min followed by centrifugation at 14,000 rpm for 5 min. Aqueous layer from the top was removed without disturbing the loose protein precipitate at the interface of aqueous and organic phase. 400 μl of methanol was added, mixed very gently, and centrifuged at 14,000 rpm for 10 min. The organic layer was discarded and the protein pellets were immediately suspended in 8 μl 100% TFA. The mixture was mixed gently and placed in an ultrasonic bath for 5 min to resuspend the pellet completely. The protein suspension was diluted to 400 μl by addition of water to a TFA concentration of 2%. Pepsin digestion was carried out after addition of freshly prepared porcine pepsin (Sigma) to the detergent free protein suspension in 2% TFA from a pepsin stock solution (1 mg/ml) at a final 1:10 w/w (Pepsin/KirBac3.1) ratio. The digestion mixture was incubated at 37°C for 4 hr. Heating at 100°C for 5 min terminated the digestion.

LC-MS and Data Analysis

The digests prepared above were analyzed by LC-MS/MS using a UltiMate 3000 LC systems (Dionex, San Francisco, CA) interfaced to a LTQ-Orbitrap XL mass spectrometer (Thermo-Finnigan, Bremen, Germany). The platform was operated in the nano-LC mode using the standard nano-ESI API stack fitted with a picotip emitter (uncoated fitting, 10 μm spray orifice; New Objective, Woburn, MA). The solvent flow rate through the column was maintained at 300 nl/min using a 1:1000 splitter system. The protein digests (1–2 pmol) were injected into a reversed-phase C18 PepMap trapping column (0.3 × 5 mm, 5 μm particle size; Dionex Inc.) equilibrated with 0.1% formic acid (FA)/2% acetonitrile (v/v) and washed for 5 min with the equilibration solvent at a flow rate of 25 μL/min, using an isocratic loading pump operated through an autosampler. After the washing step, the trapping column was switched in-line with a reversed-phase C18 Acclaim PepMap 100 column (0.075 × 150 mm; Dionex Inc.) and the peptides were eluted using a linear gradient of acetonitrile from 6% to 66% in aqueous 0.1% formic acid over a period of 60 min at the above-mentioned flow rate such that the eluate was directly introduced to the mass spectrometer. A 100% acetonitrile elution step was subsequently carried out for 5 min before resetting the analytical column to the initial equilibration conditions for another 12 min at the end of the chromatographic run. The mass spectrometer was operated in a data-dependent MS to MS/MS switching mode, with the five most intense ions in each MS scan subjected to MS/MS analysis. The full scan was carried out at 60,000 resolution in the Orbitrap detector and the MS/MS fragmentation scans were carried out in the ion trap detector CID mode such that the total scan cycle frequency was ~1 s. The threshold intensity for the MS/MS trigger was always set at 1000 and the fragmentation was carried out using the CID mode using a normalized collision energy of 35. The data was entirely collected in the profile mode for the full scan and centroid mode for the MS/MS scans. Dynamic exclusion function for previously selected precursor ions was enabled during the analysis such that the following parameters were applied: repeat count of 2, repeat duration of 45 s, exclusion duration of 60 s, and exclusion size list of 150. Xcalibur software (version 2.0.5, build 0704, Thermo-Finnigan, San Jose, CA) was used for instrument control, data acquisition, and data processing.

MS/MS spectra of the peptide mixtures (Figure S1A) were searched against manually loaded KirBac3.1 sequence in an *Escherichia coli* data base for modifications (oxidation)(Takamoto and Chance, 2006; Xu and Chance, 2007) of the peptic peptides from the KirBac3.1 protein using BioWorks 3.3 software (ThermoFisher Scientific). In addition, detected MS/MS mass spectral data for modified peptides were manually interpreted and correlated

with hypothetical MS/MS spectra predicted for the proteolysis products of the KirBac3.1 protein with the aid of the ProteinProspector (UCSF, CA) algorithm and Bioworks 3.3 software (Figure S1B). The sequence coverage and position of modified residues in the primary sequence were represented by the software Caitltu and Rapadura (Carvalho et al., 2008) (Figure S2). The total ion chromatograms were utilized to determine the extent of modification by separate quantification of the unmodified proteolytic peptides and their radiolytic products by dividing the peak area corresponding to the modified peptide by that of the total peptide peak area (modified and unmodified) (Takamoto and Chance, 2006) (Figure S1). Levels of modification versus exposure time were plotted and fitted with a single exponential function with Origin version 7.5 (OriginLabs, Northampton, MA) to determine the rate of peptide modification. The Origin program, using 95% confidence limits of the fitting results, determined the reported errors of the rate data. For mapping of the modified residues KirBac3.1 closed state PDB structure 1XL4 was used.

SUPPLEMENTAL INFORMATION

Supplemental Information includes three figures and can be found with this article online at doi:10.1016/j.str.2010.04.012.

REFERENCES

Ader, C., Schneider, R., Hornig, S., Velisetty, P., Wilson, E.M., Lange, A., Giller, K., Ohmert, I., Martin-Eauclaire, M.F., Trauner, D., et al. (2008). A structural link between inactivation and block of a K+ channel. Nat. Struct. Mol. Biol. *15*, 605–612.

Angel, T.E., Chance, M.R., and Palczewski, K. (2009a). Conserved waters mediate structural and functional activation of family A (rhodopsin-like) G protein-coupled receptors. Proc. Natl. Acad. Sci. USA *106*, 8555–8560.

Angel, T.E., Gupta, S., Jastrzebska, B., Palczewski, K., and Chance, M.R. (2009b). Structural waters define a functional channel mediating activation of the GPCR, rhodopsin. Proc. Natl. Acad. Sci. USA *106*, 14367–14372.

Berneche, S., and Roux, B. (2005). A gate in the selectivity filter of potassium channels. Structure *13*, 591–600.

Bichet, D., Haass, F.A., and Jan, L.Y. (2003). Merging functional studies with structures of inward-rectifier K(+) channels. Nat. Rev. Neurosci. *4*, 957–967.

Carvalho, P.C., Junqueira, M., Valente, R.H., and Domont, G.B. (2008). Caititu: a tool to graphically represent peptide sequence coverage and domain distribution. J. Proteomics *71*, 486–489.

Cheng, W.W., Enkvetchakul, D., and Nichols, C.G. (2009). KirBac1.1: it's an inward rectifying potassium channel. J. Gen. Physiol. *133*, 295–305.

Cordero-Morales, J.F., Cuello, L.G., Zhao, Y., Jogini, V., Cortes, D.M., Roux, B., and Perozo, E. (2006). Molecular determinants of gating at the potassium-channel selectivity filter. Nat. Struct. Mol. Biol. *13*, 311–318.

Enkvetchakul, D., Jeliazkova, I., Bhattacharyya, J., and Nichols, C.G. (2007). Control of inward rectifier K channel activity by lipid tethering of cytoplasmic domains. J. Gen. Physiol. *130*, 329–334.

Epshtein, Y., Chopra, A.P., Rosenhouse-Dantsker, A., Kowalsky, G.B., Logothetis, D.E., and Levitan, I. (2009). Identification of a C-terminus domain critical for the sensitivity of Kir2.1 to cholesterol. Proc. Natl. Acad. Sci. USA *106*, 8055–8060.

Fallen, K., Banerjee, S., Sheehan, J., Addison, D., Lewis, L.M., Meiler, J., and Denton, J.S. (2009). The Kir channel immunoglobulin domain is essential for Kir1.1 (ROMK) thermodynamic stability, trafficking and gating. Channels (Austin) *3*, 57–68.

Fraczkiewicz, R., and Braun, W. (1998). Exact and efficient analytical calculation of the accessible surface areas and their gradients for macromolecules. J. Comput. Chem. *19*, 319–333.

Guan, J.Q., and Chance, M.R. (2005). Structural proteomics of macromolecular assemblies using oxidative footprinting and mass spectrometry. Trends Biochem. Sci. *30*, 583–592.

Gupta, S., Sullivan, M., Toomey, J., Kiselar, J., and Chance, M.R. (2007). The Beamline X28C of the Center for Synchrotron Biosciences: a national resource for biomolecular structure and dynamics experiments using synchrotron footprinting. J. Synchrotron Radiat. *14*, 233–243.

Jaroslawski, S., Zadek, B., Ashcroft, F., Venien-Bryan, C., and Scheuring, S. (2007). Direct visualization of KirBac3.1 potassium channel gating by atomic force microscopy. J. Mol. Biol. *374*, 500–505.

Kiselar, J.G., Maleknia, S.D., Sullivan, M., Downard, K.M., and Chance, M.R. (2002). Hydroxyl radical probe of protein surfaces using synchrotron X-ray radiolysis and mass spectrometry. Int. J. Radiat. Biol. *78*, 101–114.

Kuo, A., Domene, C., Johnson, L.N., Doyle, D.A., and Venien-Bryan, C. (2005). Two different conformational states of the KirBac3.1 potassium channel revealed by electron crystallography. Structure *13*, 1463–1472.

Kuo, A., Gulbis, J.M., Antcliff, J.F., Rahman, T., Lowe, E.D., Zimmer, J., Cuthbertson, J., Ashcroft, F.M., Ezaki, T., and Doyle, D.A. (2003). Crystal structure of the potassium channel KirBac1.1 in the closed state. Science *300*, 1922–1926.

Nishida, M., Cadene, M., Chait, B.T., and MacKinnon, R. (2007). Crystal structure of a Kir3.1-prokaryotic Kir channel chimera. EMBO J. *26*, 4005–4015.

Pegan, S., Arrabit, C., Zhou, W., Kwiatkowski, W., Collins, A., Slesinger, P.A., and Choe, S. (2005). Cytoplasmic domain structures of Kir2.1 and Kir3.1 show sites for modulating gating and rectification. Nat. Neurosci. *8*, 279–287.

Singh, D.K., Rosenhouse-Dantsker, A., Nichols, C.G., Enkvetchakul, D., and Levitan, I. (2009). Direct regulation of prokaryotic Kir channel by cholesterol. J. Biol. Chem. *284*, 30727–30736.

Sullivan, M.R., Rekhi, S., Bohon, J., Gupta, S., Abel, D., Toomey, J., and Chance, M.R. (2008). Installation and testing of a focusing mirror at beamline X28C for high flux x-ray radiolysis of biological macromolecules. Rev. Sci. Instrum. *79*, 025101.

Swartz, K.J. (2004). Towards a structural view of gating in potassium channels. Nat. Rev. Neurosci. *5*, 905–916.

Takamoto, K., and Chance, M.R. (2006). Radiolytic protein footprinting with mass spectrometry to probe the structure of macromolecular complexes. Annu. Rev. Biophys. Biomol. Struct. *35*, 251–276.

Tao, X., Avalos, J.L., Chen, J., and Mackinnon, R. (2009). Crystal structure of the eukaryotic strong inward-rectifier k+ channel kir2.2 at 3.1 a resolution. Science *326*, 1668–1674.

Tucker, S.J., and Baukrowitz, T. (2008). How highly charged anionic lipids bind and regulate ion channels. J. Gen. Physiol. *131*, 431–438.

Xu, G., and Chance, M.R. (2007). Hydroxyl radical-mediated modification of proteins as probes for structural proteomics. Chem. Rev. *107*, 3514–3543.

Xu, G., Kiselar, J., He, Q., and Chance, M.R. (2005). Secondary reactions and strategies to improve quantitative protein footprinting. Anal. Chem. *77*, 3029–3037.

Zhu, Y., Guo, T., Park, J.E., Li, X., Meng, W., Datta, A., Bern, M., Lim, S.K., and Sze, S.K. (2009). Elucidating in vivo structural dynamics in integral membrane protein by hydroxyl radical footprinting. Mol. Cell. Proteomics *8*, 1999–2010.